Biomaterials Science: Processing, Properties, and Applications V

Edited by
Roger Narayan
Susmita Bose
Amit Bandyopadhyay

Ceramic Transactions
Volume 254

The American Ceramic Society

WILEY

Biomaterials Science: Processing, Properties, and Applications V

Biomaterials Science: Processing, Properties, and Applications V

Ceramic Transactions, Volume 254

Edited by
Roger Narayan
Susmita Bose
Amit Bandyopadhyay

The American Ceramic Society
www.ceramics.org

WILEY

Published by John Wiley & Sons, Inc., Hoboken, New Jersey.

Published simultaneously in Canada.

Library of Congress Cataloging-in-Publication Data is available.

ISBN: 978-1-119-19002-8
ISSN: 1042-1122

Contents

SURFACE PROPERTIES OF BIOMATERIALS

Preface

This volume is a collection of research papers from the Next Generation Biomaterials and Surface Properties of Biomaterials symposia, which took place during the Materials Science & Technology 2014 Conference & Exhibition (MS&T'14), at the David L. Lawrence Convention Center, Pittsburgh, Pennsylvania.
These symposia focused on several key areas, including biomaterials for tissue engineering, ceramic biomaterials, metallic biomaterials, biomaterials for drug delivery, nanostructured biomaterials, biomedical coatings, and surface modification technologies.

We would like to thank the following symposium organizers for their valuable assistance: Kalpana Katti, North Dakota State University; Mukesh Kumar, Biomet Inc; Kajal Mallick, University of Warwick; Sharmila Mukhopadhyay, Wright State University; Vilupanur Ravi, California State Polytechnic University, Pomona; and Varshni Singh, Louisiana State University. Thanks also to all of the authors, participants, and reviewers of this *Ceramic Transactions* proceedings issue.

We hope that this issue becomes a useful resource in the area of biomaterials research that not only contributes to the overall advancement of this field but also signifies the growing roles of The American Ceramic Society and its partner materials societies in this rapidly developing field.

ROGER NARAYAN, UNC/NCSU Joint Department of Biomedical Engineering
SUSMITA BOSE, Washington State University
AMIT BANDYOPADHYAY, Washington State University

Next Generation Bioceramics

EVALUATION OF LONG-TERM MECHANICAL AND BIOLOGICAL BIOCOMPATIBILITY OF LOW-COST β-TYPE Ti-Mn ALLOYS FOR BIOMEDICAL APPLICATIONS

Ken Cho, Mitsuo Niinomi, Masaaki Nakai, Pedro Fernandes Santos, Alethea Morgane Liens,
Institute for Materials Research, Tohoku University
Sendai, Miyagi, Japan

Masahiko Ikeda
Faculty of Chemistry, Materials and Bioengineering, Kansai University
Suita, Osaka, Japan

Tomokazu Hattori
Faculty of Science and Technology, Meijo University,
Nagoya, Japan

ABSTRACT

To evaluate the long-term mechanical biocompatibility of Ti-Mn alloys, the microstructures, Young's moduli, and tensile and fatigue properties of the solutionized Ti-8Mn and Ti-13Mn were investigated. In addition, to evaluate the long-term biological biocompatibility of Ti-Mn alloys, the bone formability of the solutionized Ti-12Mn implant was evaluated by animal testing. The solutionized Ti-8Mn and Ti-13Mn consist of equiaxed β-grains with diameters of approximately 420 m and 430 μm, respectively. Moreover, the solutionized Ti-8Mn also contains an athermal ω phase. The 0.2 % proof stress ($\sigma_{0.2}$), tensile strength (σ_B), and elongation of the solutionized Ti-8Mn are 1148 MPa, 1184 MPa, and 2%, respectively. The $\sigma_{0.2}$ and σ_B decrease to 915 MPa and 953 MPa, respectively, and the elongation increases to 7% for the solutionized Ti-13Mn. The higher strength and significantly lower elongation of the solutionized Ti-8Mn are attributed to precipitation of an athermal ω phase. The fatigue strength of the solutionized Ti-8Mn is comparable to that of the aged Ti-6Al-4V ELI in the low-cycle fatigue life region. The striation widths of the solutionized Ti-8Mn and Ti-13Mn are 2.4 m and 7.8 m, respectively. The smaller striation width of the solutionized Ti-8Mn indicates that the crack propagation rate in the solutionized Ti-8Mn is smaller than that in the solutionized Ti-13Mn. The relative bone contact ratio of the solutionized Ti-12Mn increases from 11% to 29% when the implant period increases from 12 to 52 weeks. The relative bone contact ratios of the solutionized Ti-12Mn implant and the commercially pure Ti implant are almost identical for all implantation periods.

INTRODUCTION

Commercially pure titanium (CP-Ti) and (α+β)-type Ti-6Al-4V ELI (Ti-64 ELI, numbers indicate mass percentage of elements) are widely used as metallic materials for biomedical applications, including artificial hip joints[1] and spinal fixation devices[2]. However, the relatively high Young's moduli of CP-Ti (105 GPa)[3] and Ti-64 ELI (110 GPa)[3] in comparison with that of cortical bone (10-30 GPa)[4] are a significant drawback. This mismatch between the Young's moduli of cortical bone and implant devices made of CP-Ti and Ti-64 ELI leads to stress shielding, which results in bone absorption and the degradation of bone quality[5]. Therefore, β-type Ti alloys with low Young's moduli, such as Ti-29Nb-13Ta-4.6Zr (TNTZ)[6], have been developed in order to overcome this drawback. The Young's modulus of TNTZ is approximately 60 GPa[6], and is much closer to that of cortical bone than that of CP-Ti and Ti-64 ELI. These β-type Ti alloys, such as TNTZ, are expected to replace CP-Ti and Ti-64 ELI in biomedical applications that require metallic biomaterials because of their low Young's moduli and good balance between strength and ductility.

However, the availability of alloying elements for these β-type Ti alloys, such as Nb and Ta, is limited. Therefore, the development of new β-type Ti alloys containing abundant alloying elements is required. Mn is a strong candidate for use as an alloying element because of its abundance; significant amounts of Mn nodules and Mn crust exist at the ocean floor. The toxicity of Mn is also lower than that of V[7]. Therefore, Mn was selected as a β-stabilizer to develop new β-type Ti alloys in this study.

For biomedical applications, metallic materials must have suitable levels of long-term mechanical biocompatibility, including wear, fatigue, and fretting fatigue properties. Moreover, their long-term biological biocompatibility, which includes bone formability, cytotoxicity, and allergic reactions, is also important. Therefore, to determine the suitability of Ti-Mn alloys for biomedical applications, their long-term mechanical and biological biocompatibility were evaluated in this study. Namely, to evaluate the long-term mechanical biocompatibility of Ti-Mn alloys, the microstructures, Young's moduli, and tensile and fatigue properties of Ti-Mn alloys were investigated. To evaluate the long-term biocompatibility, the bone formability of Ti-Mn alloys was evaluated by animal testing[8].

EXPERIMENTAL

To investigate the microstructures, tensile and fatigue properties of Ti-Mn alloys, Ti-8Mn and Ti-13Mn were fabricated by melting process under a high-purity Ar atmosphere. Ingots of Ti-8Mn and Ti-13Mn were homogenized at 1273 K for 21.6 ks, and hot-forged and hot-rolled at 1173 K. After these processes, the ingots were subjected to a stress relief treatment at 923 K for 14.4 ks followed by furnace cooling. Then, the stress-relieved ingots were subjected to a solution treatment at 1033 K for 3.6 ks followed by water quenching. The chemical compositions of the solutionized Ti-8Mn, Ti-13Mn and Ti-64 ELI[9] are listed in Table I.

Table I. Chemical compositions of Ti-8Mn, Ti-13Mn and Ti-6Al-4V ELI[9].

	Mn	Al	V	O	C	Ti
Ti-8Mn	7.9	-	-	0.100	0.0085	Bal.
Ti-13Mn	12.8	-	-	0.105	0.0050	Bal.
Ti-6Al-4V ELI[9]	-	5.75-6.50	3.50-4.50	<0.15	<0.08	Bal.

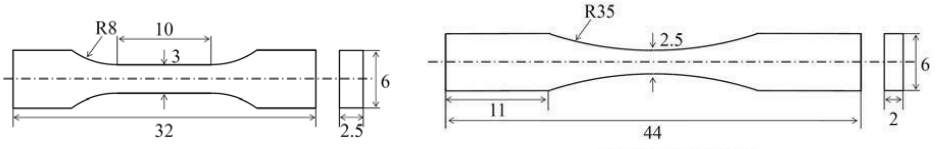

(a) Tensile specimen (b) Fatigue specimen

Figure 1. Geometry of (a) tensile and (b) fatigue specimens.

The microstructures of the solutionized Ti-8Mn and Ti-13Mn were evaluated with optical microscopy (OM). For OM observations, the solutionized Ti-8Mn and Ti-13 Mn were etched using a 5% HF and 6% HNO_3 etching solution. The phase constituents of the solutionized Ti-8Mn and Ti-13Mn were investigated with X-ray diffraction analysis (XRD) and transmission electron microscopy (TEM).

The Young's moduli of the solutionized Ti-8Mn and Ti-13Mn were measured using a free resonance method.

The tensile properties of the solutionized Ti-8Mn and Ti-13Mn were evaluated at room temperature in air using an Instron-type testing machine with a crosshead speed of 8.33×10^{-6} $m \cdot s^{-1}$. Figure 1 (a) shows the geometry of the tensile specimens.

The fatigue properties of the solutionized Ti-8Mn and Ti-13Mn were evaluated using an electro-servo-hydraulic testing machine. The fatigue tests were performed at room temperature in air at a frequency of 10 Hz with a stress ratio (R) of 0.1 under the tension–tension mode. The maximum cyclic stress at which the fatigue specimen did not fail after 1×10^6 cycles was defined as the plain fatigue limit (run out). Figure 1 (b) shows the geometry of the fatigue specimens. The fracture surfaces were observed using a scanning electron microscopy (SEM).

To investigate the bone formability of the Ti-Mn alloys using an animal testing, Ti-12Mn was used for the implant. The bone formability of metallic materials is affected by the metallic ions released in human or animal body from the metallic materials and the properties of oxide layer on the surface of metallic materials. Cho et al. has reported the amounts of Ti and Mn ions released in 1 % lactic acid solution from Ti-(6-13)Mn[10]. The amounts of Ti and Mn ions released in 1% lactic acid solution from Ti-8Mn and Ti-13Mn is smaller than or the same as those released from Ti-12Mn[10]. Moreover, the addition of Mn does not show any significant effects on the properties of Ti oxide layer on the surface of Ti-(6-13)Mn alloys[10]. Therefore, solutionized

Ti-12Mn was used for the implant in this study.

The Ti-12Mn was fabricated by melting process under a high-purity Ar atmosphere. An ingot of Ti-12Mn was homogenized at 1273 K for 43 ks, and then hot-forged at 827 K. After these processes, the ingot was subjected to a solution treatment at 1033 K for 3.6 ks. For the animal testing, implants with a diameter of 5 mm and a length of 10 mm were machined from the solutionized Ti-12Mn and CP-Ti for comparison. They were sterilized with steam under a pressure of 0.2 MPa at 394 K for 0.9 ks, and then implanted into the femoral bones of Japanese white house rabbits in a surgical procedure. After 12, 52, and 96 weeks from implantation, the femoral bones containing the implants were removed. The bone formability of the implants was evaluated using a contact microradiography (CMR).

RESULTS AND DISCUSSION

Figure 2 shows typical OM images of the solutionized Ti-8Mn and Ti-13Mn. The solutionized Ti-8Mn and Ti-13Mn consist of equiaxed grains. The grain diameters for the solutionized Ti-8Mn and Ti-13Mn were estimated to be 420 μm and 430 μm, respectively.

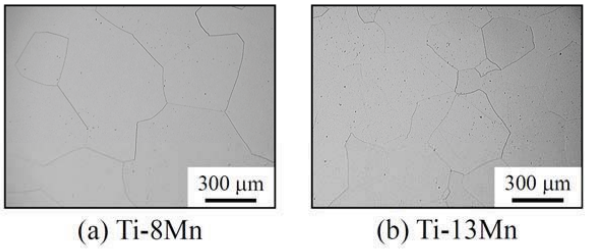

Figure 2. Typical OM images of solutionized (a) Ti-8Mn and (b) Ti-13Mn.

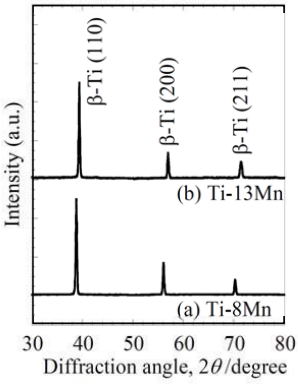

Figure 3. Typical XRD profiles of solutionized (a) Ti-8Mn and (b) Ti-13Mn.

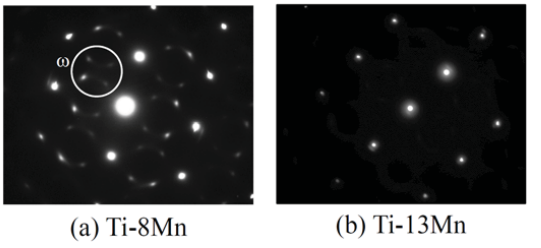

Figure 4. Typical SAED patterns of solutionized (a) Ti-8Mn and (b) Ti-13Mn.

Typical XRD profiles of the solutionized Ti-8Mn and Ti-13Mn alloys are shown in Fig. 3. The profiles were normalized using an intensity of the β (110) peak. Only diffraction peaks attributable to the β (110), β (200), and β (211) planes are detected. This result indicates that the solutionized Ti-8Mn and Ti-13Mn consist of a β phase. Figure 4 shows typical selected-area electron diffraction (SAED) patterns of the solutionized Ti-8Mn and Ti-13Mn. Weak circular diffuse streaks attributed to an athermal ω phase are observed for solutionized Ti-8Mn as shown in Fig. 4 (a). On the other hand, only diffraction spots attributed to the β-phase are observed for solutionized Ti-13Mn. The athermal ω phase disappears with increasing Mn content because the β stability increases with increasing Mn content.

The Young's moduli of the solutionized Ti-8Mn and Ti-13Mn were 88 GPa and 94 GPa, respectively. The Young's moduli of the solutionized Ti-8Mn and Ti-13Mn are lower than that of aged Ti-64 ELI. It is well known that the Young's modulus of ω phase is higher than that of β phase. As above-mentioned, The athermal ω phase disappears with increasing Mn content. However, the solutionized Ti-8Mn, in which the athermal ω phase exists, shows the lower Young's modulus compared with the solutionized Ti-13Mn. Therfore, it is supposed that the effect of solid solution of Mn is dominant for Ti-13Mn.

Figure 5 shows the 0.2% proof stress, $\sigma_{0.2}$, ultimate tensile strength, σ_B, and elongation of the solutionized Ti-8Mn and Ti-13Mn, along with those of aged Ti- ELI[9]. The $\sigma_{0.2}$ and σ_B of the solutionized Ti-8Mn is 1148 MPa and 1184 MPa, respectively, which are higher than those of aged Ti-64 ELI ($\sigma_{0.2}$: 780 MPa and σ_B: 900 MPa)[11]. The $\sigma_{0.2}$ and σ_B of the solutionized Ti-13Mn decrease to 915 MPa and 953 MPa, respectively, while the elongation increases from 2% to 7% as compared with those of the solutionized Ti-8Mn. The higher strength and significantly lower elongation for the solutionized Ti-8Mn as compared with the solutionized Ti-13Mn are attributed to precipitation of an athermal ω phase.

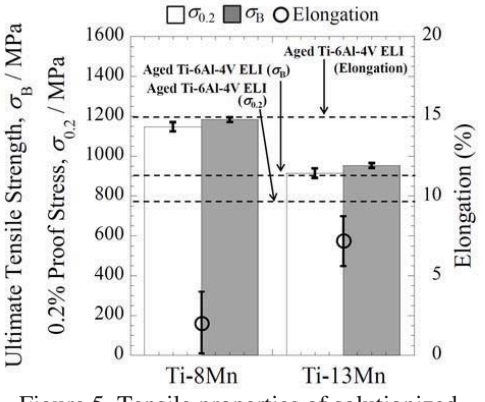

Figure 5. Tensile properties of solutionized Ti-8Mn and Ti-13Mn, along with those of aged Ti-6Al-4V.

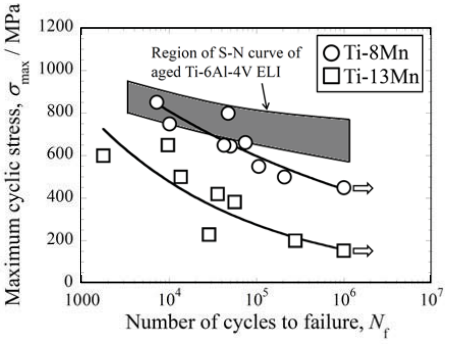

Figure 6. *S-N* curves of solutionized Ti-8Mn and Ti-13Mn along with region of that of aged Ti-6Al-4V ELI[12].

Maximum cyclic stress, (σ_{max}, S), against the number of cycles to failure (N) curves, that is, S–N curves, obtained for the solutionized Ti-8Mn and Ti-13Mn are shown in Fig. 6. For comparison, the region of S-N curves for aged Ti-64 ELI[12] is also shown in Fig. 6. The fatigue strength of the solutionized Ti-8Mn is higher than that of the solutionized Ti-13Mn. In addition, the fatigue strength of the solutionized Ti-8Mn in the low-cycle fatigue life region is comparable to that of the aged Ti-64 ELI.

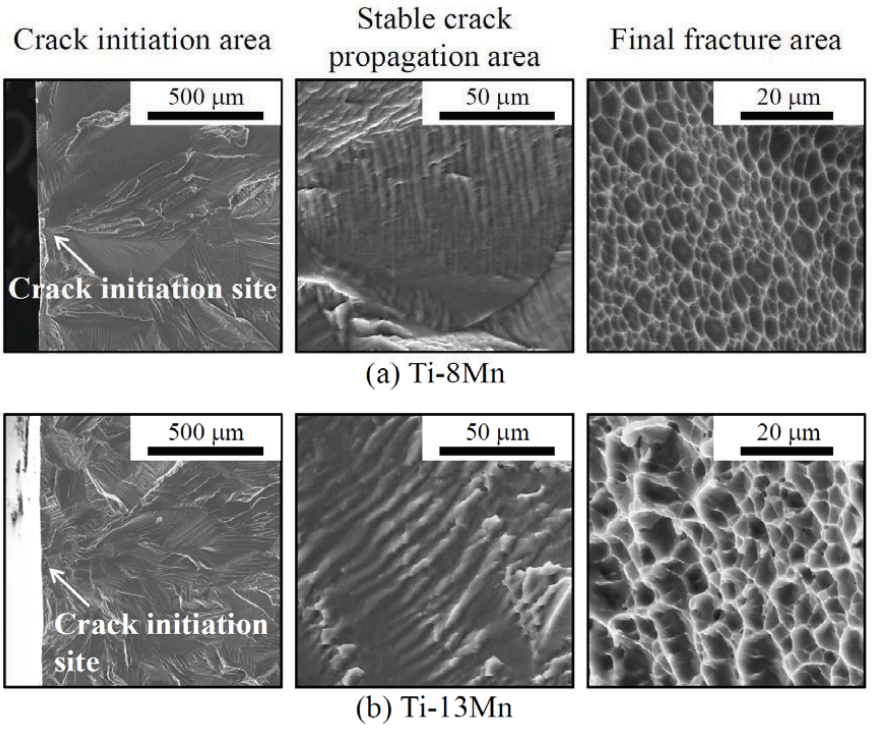

Figure 7. SEM fractographs of crack initiation areas, stable crack propagation areas, and final fracture areas of (a) Ti-8Mn and (b) Ti-13Mn.

Figure 7 shows the fatigue fracture surfaces of the solutionized Ti-8Mn and Ti-13Mn tested at σ_{max} = 500 MPa. For both solutionized Ti-8Mn and Ti-13Mn, the crack initiation site is at the surface. The fractographs of the stable crack propagation areas of the solutionized Ti-8Mn and Ti-13Mn observed at 1.4 mm and 1.5 mm from each crack initiation site are shown in Fig. 7. The average striation widths of the solutionized Ti-8Mn and Ti-13Mn are 2.4 μm and 7.8 μm, respectively. The smaller striation width of the solutionized Ti-8Mn indicates that the crack propagation rate in the solutionized Ti-8Mn is lower than that in the solutionized Ti-13Mn. It is supposed that the difference in crack propagation rate between the solutionized Ti-8Mn and Ti-13Mn is caused by the presence of an athermal ω phase. The dimples on the fracture surface at the

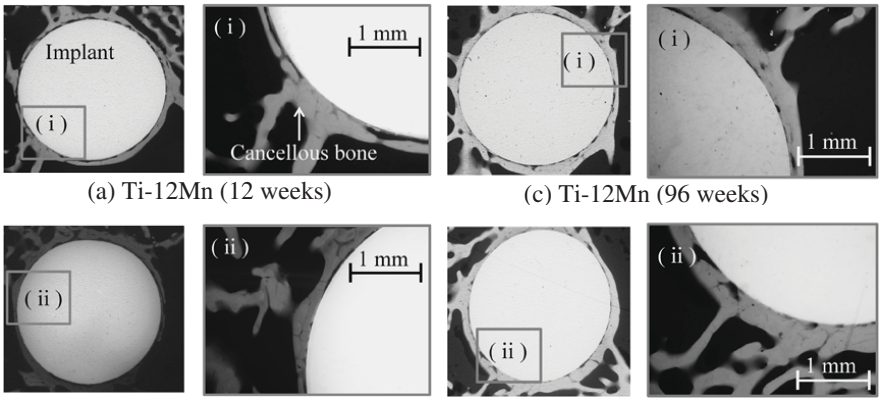

(a) Ti-12Mn (12 weeks) (c) Ti-12Mn (96 weeks)

(b) CP-Ti (12 weeks) (d) CP-Ti (96 weeks)

Figure 8. CMR images of cross-sections of the implants: (a) solutionized Ti-12Mn implant and (b) CP-Ti implant at 12 weeks, and (c) solutionized Ti-12Mn implant and (d) CP-Ti implant at 96 weeks after implantation[8].

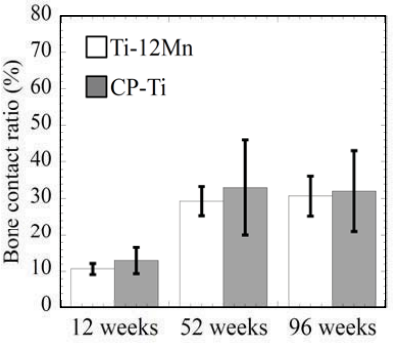

Figure 9. Relative bone contact ratios of solutionized Ti-12Mn implant and CP-Ti implant at 12, 52, and 96 weeks after implantation[8].

final fracture area of the solutionized Ti-8Mn are smaller and shallower than those on the fracture surface at the final fracture area of the solutionized Ti-13Mn because the ductility of the solutionized Ti-8Mn is inferior to that of the soliutionized Ti-13Mn. The ductility of Ti-8Mn is reduced due to the precipitation of the athermal ω phase.

Cross-sectional CMR images of the implanted solutionized Ti-12Mn and CP-Ti implants at 12 and 96 weeks after implantation are shown in Fig. 8[8]. Each alloy implant is surrounded by newly formed bone tissue, and a large portion of this tissue is in direct contact with each alloy as shown in Fig. 8. The thickness of the newly formed bone tissue and the area of the bone tissue in direct contact with the each alloy increase significantly with increasing implantation period. The relative bone contact ratios of the solutionized Ti-12Mn and CP-Ti implants at 12, 52, and 96 weeks after implantation are summarized in Fig. 9[8]. The relative bone contact ratios of the

solutionized Ti-12Mn and CP-Ti implants increase from 11% to 29% and from 13% to 33%, respectively, when implant period is increased from 12 to 52 weeks. On the other hand, the relative bone contact ratio at 96 weeks after implantation is almost equal for that at 52 weeks after implantation for both the solutionized Ti-12Mn and CP-Ti implants: they are 31 % and 32 % for the solutionized Ti-12Mn and CP-Ti implants. These results indicate that the formation of new bone tissue does not significantly change with implant period longer than 52 weeks. In addition, the relative bone contact ratios of the solutionized Ti-12Mn and CP-Ti implants are almost equal for all implantation period.

The results obtained from tensile and fatigue tests suggest that the long-term mechanical biocompatibility, especially the tensile strength of the solutionized Ti-8Mn and Ti-13Mn, and the the fatigue strength of the solutionized Ti-8Mn in low-cycle fatigue life region are comparable to that of aged Ti-64 ELI. However, the elongation and the fatigue strength in the high-cycle fatigue life region of the solutionized Ti-8Mn and Ti-13Mn are required to be improved. On the other hand, the animal testing suggests that the long-term biological biocompatibility, which is the bone formability, of the solutionized Ti-12Mn implant is similar to that of the CP-Ti implant.

The bone formability of metallic materials is mainly affected by the metallic ions released from the metallic materials and the properties of oxide layer on the surface of metallic materials. The amounts of Ti and Mn ions released in 1% lactic acid solution from Ti-8Mn and Ti-13Mn is smaller than or the same as those released from Ti-12Mn[10]. Moreover, the addition of Mn does not show any significant effects on the properties of Ti oxide layer on the surface of Ti-(6-13)Mn alloys[10]. Therefore, it is expected that there are no significant differences in the bone formability between solutionized Ti-12Mn and solutionized Ti-8Mn and Ti-13Mn .

CONCLUSIONS

To evaluate the long-term mechanical biocompatibility of Ti-Mn alloys, the microstructures, and tensile and fatigue properties of the solutionized Ti-8Mn and Ti-13Mn were investigated. In addition, to evaluate the long-term biological biocompatibility of the Ti-Mn alloys, the bone formability of the solutionized Ti-12Mn implant was investigated by animal testing.

1. The solutionized Ti-8Mn and Ti-13Mn consists of equiaxed β-grains with diameters of approximately 420 μm and 430 μm, respectively.
2. An athermal ω phase exists in the solutionized Ti-8Mn, but it is not found in the solutionized Ti-13Mn.
3. The Young's moduli of the solutionized Ti-8Mn and Ti-13Mn were 88 GPa and 94 GPa, respectively. The Young's moduli of the solutionized Ti-8Mn and Ti-13Mn are lower than that of aged Ti-64 ELI.
4. The $\sigma_{0.2}$, σ_B, and elongation of solutionized Ti-8Mn is 1148 MPa, 1184 MPa, and 2%, respectively. The $\sigma_{0.2}$ and σ_B decrease to 915 MPa and 953 MPa, respectively and the

elongation increases to 7% for the solutionized Ti-13Mn.

5. The fatigue strength of the solutionized Ti-8Mn is higher than that of the solutionized Ti-13Mn. Moreover, the fatigue strength of the solutionized Ti-8Mn is comparable to that of the aged Ti-64 ELI in the low-cycle fatigue life region.
6. The relative bone contact ratio of the solutionized Ti-12Mn implant increases from 11% to 29% when the implant period increases from 12 to 52 weeks. In addition, the relative bone contact ratios of the solutionized Ti-12Mn implant and the CP-Ti implant are almost identical for all implantation periods.

ACKNOWLEDGEMENT

This study was supported in part by a Grant-in-Aid for Scientific Research (A) No. 24246111, a Grant-in-Aid for Young Scientists (B) No. 25820367 from the Japan Society for the Promotion of Science (JSPS), the Inter-University Cooperative Research Program "Innovation Research for Biosis-Abiosis Intelligent Interface" from the Ministry of Education, Culture, Sports, Science and Technology (MEXT), Japan, Inamori Grants from the Inamori Foundation, Japan, and a Titanium Research Grant from the Japan Titanium Society.

REFERENCES

[1] M. Semlitsch, Titanium alloys for hip joint replacements, *Clin. Mater.*, **2**, 1-13 (1987).

[2] F. B. Christensen, M. Dalstra, F. Sejling, S. Overgaard and C. Bünger, Titanium-alloy enhances bone-pedicle screw fixation: mechanical and histomorphometrical results of titanium-alloy versus stainless steel, *Europ. Spine J.*, **9**, 97-103 (2000).

[3] M. Niinomi, Mechanical properties of biomedical titanium alloys, *Mater. Sci. Eng. A*, **243**, 231-6 (1998).

[4] M. Niinomi, Mechanical biocompatibilities of titanium alloys for biomedical applications, *J. the Mechanical Behavior of Biomedical Materials*, **1**, 30-42 (2008).

[5] R. Huiskes, H. Weinans and B. van Rietberge, The relationship between stress shielding and bone resorption around total hip stems and the effects of flexible materials, *Clin. Orthopaedics and Related Res.*, **274**, 124-34 (1992).

[6] D. Kuroda, M. Niinomi, M. Morinaga, Y. Kato and T. Yashiro, Design and mechanical properties of new β type titanium alloys for implant materials, *Mater. Sci. Eng.*, **A243**, 244-9 (1998).

[7] S. Takeda, H. Kakiuchi, H. Doi and M. Nakamura, Cytotoxicity of pure metals, *Japanese J. Dent. Mater.*, **8**, 648-52 (1989).

[8] K. Ishikura, T. Hattori, T. Akahori and M. Niinomi, Mechanical properties and biocompatibility of low cost-type Ti-Mn system binary alloys for biomedical applications, *J. Japan Inst. Met. Mater.*, **77**, 253-8 (2013).

[9] ASTM International standard: ASTM F136.